Chapter-2: Synthesis, Characterization and Analysis…

2.1 Overview

In order to complete the objective given in chapter 1, it is necessary to synthesize the investigated system and characterized them for the further analysis. In this chapter, a detailed of synthesis of materials, their characterization with different equipment and the employed experimental techniques, have been described. In the present investigations, the proposed various compositions (a) Lanthanum aluminate, $LaAlO_3$ (b) Co-doped lanthanum aluminate i.e., $La_{0.9}Sr_{0.1}Al_{0.9}Mg_{0.1}O_{3-\delta}$ (LSAM) (c) Double doped lanthanum aluminate having larger ionic radii with Ba substitution, i.e., $La_{0.9-x}Sr_{0.1}Ba_xAl_{0.9}Mg_{0.1}O_{3-\delta}$ (LSBAM, x = 0.01, 0.03, 0.05 and 0.07) and (d) Double doped lanthanum aluminate having smaller ionic radii with Sm substitution, i.e., $La_{0.9-x}Sr_{0.1}Sm_xAl_{0.9}Mg_{0.1}O_{3-\delta}$ (LSSAM, x=0.01, 0.03 and 0.05) has been prepared by citrate-nitrate auto combustion method and also to get thin electrolyte, tape casting techniques has been employed for one of the chosen composition. The system $La_{1.x}Sr_{0.1}Ba_xAl_{0.9}Mg_{0.1}O_{3-\delta}$ for x=0.01 was prepared by tape casting technique. Structural, thermal and electrical properties were analyzed of all prepared compositions. This chapter has been divided into three sections:

(1) Synthesis methods (sample preparation and processing of compositions),

(2) Characterization techniques (structure, microstructure, thermal and electrical), and

(3) Data analysis techniques (like X-ray Rietveld refinement, electrical conductivity and impedance spectroscopy).

2.2 Synthesis and Processing of the Compositions

High purity raw materials of these investigated compositions were used for synthesis process. The specifications of these materials are listed in Table 2.1.

Table 2.1: Specifications of the proposed materials

S. No.	Raw Materials	Chemical Formula	Purity	Manufacturer
1.	Lanthanum Oxide	La_2O_3	99 %	Alfa Aesar
2.	Strontium Nitrate	$Sr\ (NO_3)_2$	99 %	Alfa Aesar
3.	Aluminium Nitrate	$Al\ (NO_3)_3.6H_2O$	98%	Alfa Aesar
4.	Barium Nitrate	$Ba\ (NO_3)_2$	99%	Alfa Aesar
5.	Magnesium Nitrate	$Mg\ (NO_3)_2.6H_2O$	98%	Alfa Aesar
6.	Citric acid	$C_6H_8O_7.\ H_2O$	99%	Alfa Aeser

A few other high grade chemicals, solvent and reagents like acetone, nitric acid, hydrochloric acid, polyvinyl alcohol, plasticizer, defoaming agent, ammonia solution, Myler film etc. were also used to fabricate the samples.

2.3 Synthesis of Materials

In order to synthesize the investigated system various techniques have been explored to synthesize Lanthanum aluminate powders. Some of them are: solid state ceramic route, flash combustion, urea based homogeneous precipitation, hexamethylenetetramine based homogeneous precipitation, sol-gel, thermal decomposition, hydrothermal synthesis, micro emulsion method, spray hydrolysis reaction method, etc. All these methods have their own merits and demerits. In the solid state ceramic processes, high sintering temperature (~1600 °C) is required for densification which is not economical and can allow lanthanum aluminate to be lost due to high mobility of La^{3+} at these temperatures. Thermal decomposition and flash combustion methods give large agglomerates of nearly 10 μm, and difficult to synthesize nano-size powder. Also spray hydrolysis reaction method produces micro-size spherical

powder. Sol-gel and precipitation methods require high calcination temperature (>1000 °C) and additional treatment of grinding is necessary to obtain nano-size powder. Hydrothermal technique requires long heat treatment for several hours because of the slow reaction rate. Micro emulsion method limits the industrial production due to low yield rate. Among the available wet chemical process, combustion technique is capable of producing ultra fine powders of oxide ceramics in shorter time and at a lower calcination temperature [62], with improved powder characteristics. The success of this process is due to an intimate blending among the constituents using suitable fuel or complexing agents (e.g. glycin, citric acid, urea and so forth) in an aqueous medium followed by an exothermic redox reaction between fuel and oxidizer (i.e. Nitrates). Auto ignition, once initiated, is then self sustaining. The rapid evolution of large volume of gases during the combustion dissipates the heat of combustion and limits the rise of temperature, thus reducing the possibility of premature local partial sintering among the primary particle. It has also been seen that for the synthesis of lanthanum aluminate by citrate-nitrate auto combustion process, a constant citrate to nitrate ratio (C/N) of 0.4 was observed to be optimum to induce a self propagating and controlled autoignition reaction. In the light of these techniques citrate-nitrate auto combustion method is relatively simple and cheap process to synthesize nano-size powder.

2.3.1 Citrate-Nitrate Auto-Combustion Method

Self-propagating high temperature synthesis (SHS) also known as auto combustion is an important technique widely used for the synthesis of a variety of metal nitrates for different applications. This method has some advantages over other methods like solid state reaction method, sol-gel process, ultrasonic spray pyrolysis technique etc. which is given below

(1) The required reagents are simple compounds,

(2) There is no need for special equipment,

(3) Dopants can be easily introduced into the final product, and

(4) An agglomeration of powders remains limited,

(5) 20-50 nm size nanoparticles can synthesize,

(6) Less time and least cost process and

(7) Neither inert gas nor vacuum is required

In the combustion mixture, nitrates and organic compounds behave like conventional oxidants and fuels. First, La_2O_3 was dissolved in dilute HNO_3 and the solution was kept on a hot plate at 200 °C till crystals of La $(NO_3)_3.6H_2O$ appeared. Then this prepared lanthanum nitrate was dissolved in distilled water with other nitrate solutions to get the homogenous mixture. Ammonia solution was used to achieve a particular pH value for proper combustion. The value of the pH is maintained at 6 to avoid phase segregation and to provide a true homogeneous distribution of all the cations at the atomic level. The solution formed with all precursors was heated to evaporate water on a hot plate in the temperature range 160-200ºC with the help of magnetic stirrer bar which gave thick gel. The formed gel slowly foamed, swelled, and finally burnt on its own on a hot plate. The dark gray voluminous power (ash) was formed within few seconds. Exothermicity of combustion is controlled by the nature of the fuel and the ratio of oxidizer to fuel. Then the aqueous solution of citric acid was added to keep citrate-nitrate ratio (C/N) equal to 0.4. As prepared ash was grounded in an agate mortar and calcined in a platinum crucible at 400 °C (as per DTA and TGA curve) for 4 hours with a heating rate of 5 °C/min. This powder was grounded and pressed uniaxially under an optimum load of 7 kg/m^2 to form cylindrical pellets having a thickness in the range 1-2 mm and diameter 12 mm using a hydraulic press. For sintering, pellets were kept in a platinum crucible, covered with a platinum lid. These pellets were sintered at 1300 °C for 8 hours in the air.

Thereafter, the temperature was raised to a required sintering temperature at a rate of 5 °C/min, kept at this temperature for a required soaking period and then cooled to room temperature at a rate of 5 °C/min. A flow chart of auto combustion synthesis techniques is shown in the Fig. 2.1.

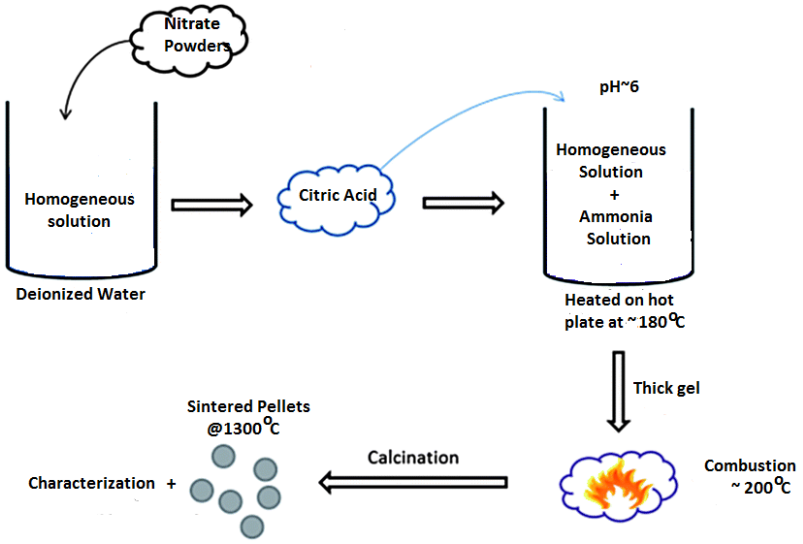

Figure 2.1: Flow chart of auto-combustion synthesis

2.3.2 Tape Casting Technique

The prime requisite in the fabrication of electrolyte system is that it should be as thin as possible with high oxide ion conductivity. Among various techniques, tape casting is relatively good method to produce thin, flat tape with a thickness between 0.1-1000 µm. For the formation of slurry in an aqueous medium variety of water soluble binder, plasticizers and dispersants is restricted in comparison to non-aqueous method. In order to prepare slurry, the amount of solvent must be fixed at the minimum to maintain homogenous slurry. The dispersant amount must be least in order to maintain stability of slurry. The plasticizer to binder ratio must be adjusted so that the tape should be flexible, resistant and easy to release. The processing technique is illustrated in Fig. 2.2. First, calcined powder is milled by ball milling using ethanol (absolute) as solvent medium and

alumina as grinding media. After milling, powder is dried in oven at 100 °C for 24 hrs. The ceramic powder has been mixed with the optimized amount of dispersant (1.57 gm) and deionised water and then again ball milled for 24 hrs. The binder and plasticizer are added into the dispersed slurry and again ball milled for 24 hours. It has been used PVA and glycerol as a binder and plasticizer, respectively. Defoaming agent, BYK-034, (Octanal) has been added to remove any entrapped air bubbles. After that vacuum degassing has been carried out prior to casting slurry. The slurry has been casted on a mylar film using a ceramic tape casting equipment (EPH Engineering Associates Inc, ELKO, USA) with a double doctor blade and stationary glass plate. Casting of the slurry has been carried out on a mylar sheet with a speed of 10 cm/min by using doctor blade with a gap of 300-375 µm. The casted ceramic tape has been dried overnight at ambient conditions and further kept in oven for drying at 150 °C for 24 hrs. In this way prepared green ceramic tape has been kept for sintering at 1350 °C. The thickness of the sintered tape has measured with screw gauge and found to be 100 µm. Initially, green tape is heated to remove the organics additives for 1 hour at 1000 °C with a heating rate of 1 °C/min up to 500 °C and 2 °C/min from 500 °C to 1000 °C and afterwards the temperature 1350 °C was achieved with a heating rate of 5 °C/min.

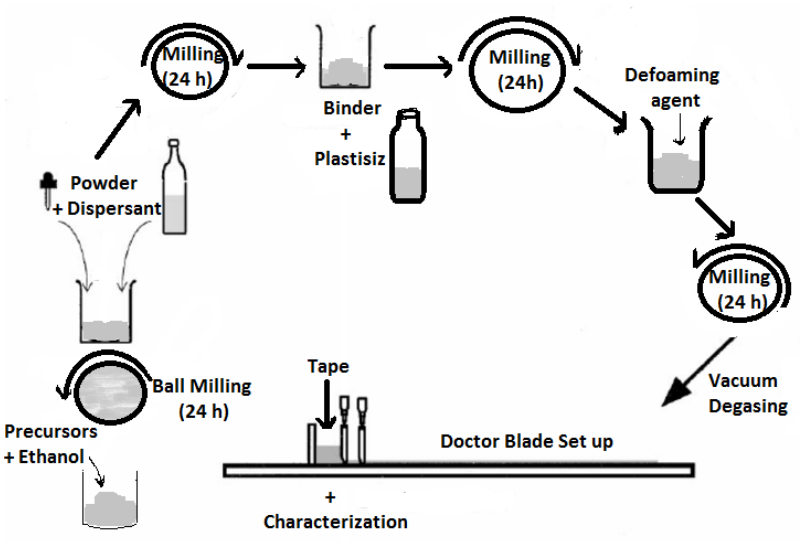

Figure 2.2: Flow chart of tape casting technique

2.4 Various Characterizations

2.4.1 Differential Thermal Analysis (DTA) and Thermo Gravimetric Analysis (TGA)

Differential thermal analysis (DTA) (Fig. 2.3) is a technique which involves heating or cooling of a test sample and an inert reference sample under identical conditions and records temperature difference which develops between them. In this method, the testing material is in the form of fine powder placed in a small capsule, often of alumina or other suitable refractory material. Adjacent to the test sample, a second capsule containing an inert powder such as α-Al_2O_3, which does not exhibit endothermic or exothermic effects, is placed. End points of thermocouple are embedded in the test substance and in the α-Al_2O_3 powder so that their e.m.f. are opposed and the net e.m.f therefore represents the temperature difference between the sample powder and the inert α-Al_2O_3. The two capsules are heated at a constant rate and the temperature difference is plotted either against time or against the temperature at some fixed points within the apparatus. There are two possibilities: first, any physical or chemical change occurring to the test sample, which involves the evolution of heat, will cause its temperature to rise temporarily above that of reference sample leading to an exothermic peak. Second, which is accompanied by the absorption of heat, will cause the temperature of the test sample to lag behind that of the reference sample, leading to an endothermic peak. The area under any given peak can be used as a quantitative measure of the amount of heat evolved or absorbed by the physical or chemical changes, which occurred.

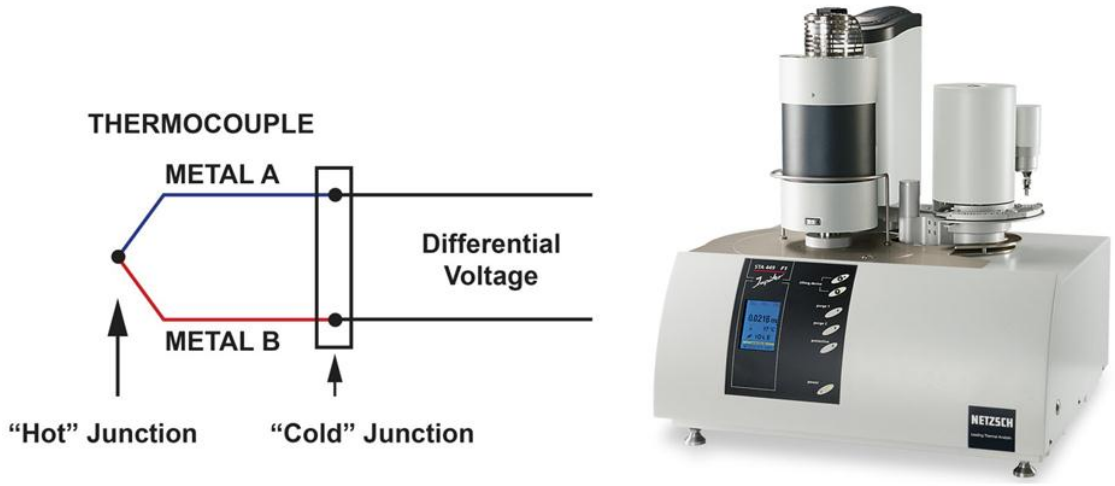

Figure 2.3: Mechanism (left) and experimental setup (right) of DTA/TGA [Ref: Netzsch-thermal-analysis.com]

Thermo gravimetric analysis (TGA) is a technique for measuring the change in weight of a substance as a function of temperature or time. The sample usually a few milligrams in weight is heated at a constant rate in the range of (1-20) °C min^{-1} and has a constant weight until it begins to decompose at a certain temperature. Under dynamic heating decomposition occurs over a range of temperature and after certain temperature no weight loss is observed leading to the completion of decomposition reaction. The weight losses are fundamental properties of the sample and can be used for quantitative calculations of compositional changes etc.

2.4.2 Powder X-Ray diffraction

X-ray diffraction (XRD) is a versatile, non-destructive technique that reveals detailed information about the crystallographic structure of natural and manufactured materials. X-ray radiations most commonly used are that emitted by copper, whose characteristic wavelength for the K_α radiation is =1.5418Å. When the incident beam strikes a powder sample, diffraction occurs in every possible orientation of 2θ. The diffracted beam may be detected by using a movable detector such as a Geiger counter, which is connected to a chart recorder. For a crystal of given inter-planar spacing (d) and

wavelength λ, the various orders n of reflection occurs only at a precise angle θ, which satisfies the Bragg condition: $2d\sin\theta = n\lambda$. The mechanism and schematic diagram of X-ray diffractometer is shown in Fig. 2.4. In normal use, the counter is set to scan over a range of 2θ values at a constant angular velocity. Routinely, a 2θ range of 20 to 80 degrees is sufficient to cover the most useful part of the powder pattern. Based on the principle of XRD, a wealth of structural, physical and chemical information about the material investigated can be obtained.

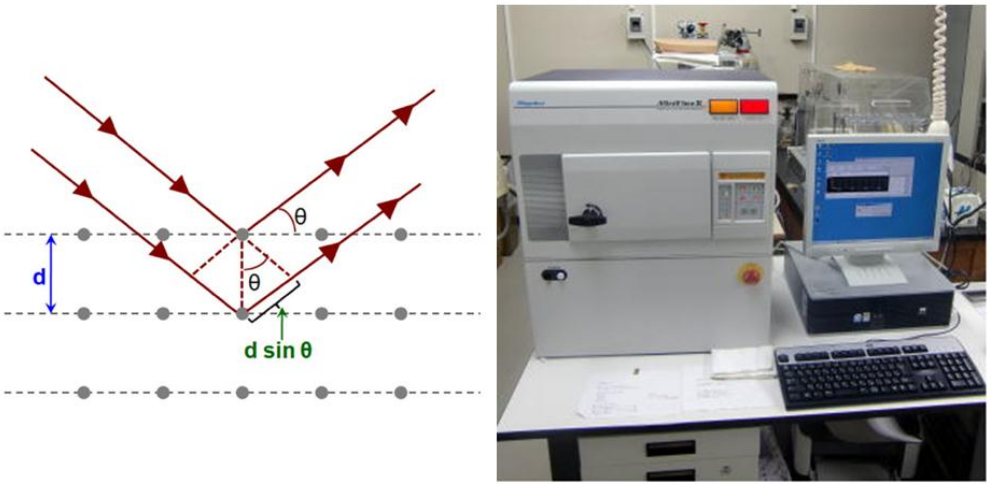

Figure 2.4: Mechanism (left) and experimental setup (right) of X-ray diffraction [Rikagu, Miniflex II]

The identification of single or multiple phases in an unknown sample is the main application of X-ray powder diffractometry. Phase identification helps us to understand the mechanism of formation of these samples.

To check the single phase formation, powder XRD was done at different stages (i.e. as burnt ash, calcined and sintered) of synthesis. The powder of as burnt ash, calcined and sintered pellets were ground and powder XRD patterns were recorded using an X-ray Diffractometer (Rigaku Miniflex II, desktop) employing Cu-Kα radiation with Ni filter. The formation of single-phase solid solution was confirmed by the absence of characteristic lines of constituent oxides or any other compounds between them in the XRD patterns. The XRD patterns were indexed and lattice parameters were determined

using non-linear least square fitting of the data using a software program 'Unit Cell'. The crystallite size was estimated by X-ray line broadening analysis. The basic information obtain from the XRD is about the structural, physical and chemical part of the system.

2.4.3 Density and Porosity Measurements

Experimental densities of the sintered pellets were determined using balance with the attached density kit (Sartorius, BSA2245CW) based on the Archimede's principle shown in Fig. 2.5.

Figure 2.5: Balance with density kit [Sartorius, BSA2245CW]

The Archimede's principal is given by

$$D = \frac{w_1}{w_2} \times \rho \qquad 2.1$$

where, D is the density of object, ρ is the density of water, W_1 & W_2 are the weight of the object and the weight of displaced water, respectively. Theoretical density was determined from the molecular weight of the compound and lattice parameters using the relation

$$D_{th} = \frac{n \times M}{N \times V} \qquad 2.2$$

where, D_{th}, n, M, N and V are theoretical density, number of formula unit per unit cell, molecular weight of the sample, Avogadro's Number and unit cell volume respectively. Percentage porosity was calculated using the relation

$$\% \text{ Porosity} = \frac{D_{th} - D_{exp}}{D_{th}} \times 100 \qquad 2.3$$

where, $D_{th.}$ and D_{exp} are theoretical density and experimental density respectively.

2.4.4 Transmission Electron Microscopy (TEM)

In TEM (Fig. 2.6 a), a beam of electron is transmitted through an ultrafine thin sample, interacting with the sample as they pass through. An image is formed from the interaction of the electrons transmitted through the sample, which is magnified and focused onto an imaging device, such as a fluorescent screen and to be detected by a sensor such as a CCD camera. TEM is capable of imaging at a significantly higher resolution because of the small de Broglie wavelength of the electron. At low magnification TEM image contrast is due to absorption of electrons in the sample, due to the thickness and composition of the sample. This technique is used to observe modulation in chemical identity, crystal orientation, electronic structure and sample induced electron phase shift as well as the regular absorption based imaging.

The most common mode of operation for TEM is the bright field imaging mode. In this mode the contrast formation is due to occlusion and absorption of electrons in the sample (classically). Thicker regions of the sample or region with higher atomic number will appear dark, whilst regions with no sample in the beam path will appear bright (hence the term bright field). High-resolution transmission electron microscopy (HRTEM) is another imaging mode of the transmission electron microscope that allows

the imaging of the crystallographic structure of a sample at an atomic scale. Because of its high resolution, it is used to study nanoscale properties of crystalline materials. Against conventional microscopy, HRTEM does not use amplitudes, i.e. absorption by the sample, for image formation. Instead, contrast arises from the interference in the image plane of the electron waves itself. Selected area electron diffraction (SAED or SAD) is a crystallographic experimental technique that can be performed inside a transmission electron microscope. In this case, electrons are treated as wave not like a particle. Since the wavelength of high energy electron is a fraction of a nanometer and the spacing between atoms in a solid is only slightly larger, the atoms act as a diffraction grating to the electron, which are diffracted. As a result, the image on the screen of the TEM will be a series of spots (selected area diffraction pattern, SADP) and each spot correspond to a satisfied diffraction condition of the sample's crystal structure. If the sample is tilted, the same crystal will stay under illumination, but different diffraction conditions will be satisfied and different diffraction spots will appear or disappear. For thin crystalline samples, this produces an image that consists of a series of dots in the case of a single crystal, or a series of rings in the case of a polycrystalline sample. For the single crystal case, the diffraction pattern is dependent upon the orientation of the sample. This image provides information about the space group symmetries in the crystal and the crystal orientation to the beam path.

To examine morphology of the as-prepared ash and calcined powder of some samples, transmission electron microscopy was done using TECHNAI G^2 20G TWIN, ultra high vacuum transmission electron microscope. For this, powder of the sample was milled in ultrasonic miller for about 3 hrs. The suspension of the particles was obtained and thereafter 2 drops of suspension were poured on copper grids (Fig. 2.6 b) (50 micron thick) and dried for an hour. Then samples were mounted on sample holder and

transferred to the TEM column. Morphology and crystal structure were investigated by using real space imaging that is the bright field TEM mode and reciprocal space imaging by selected area electron diffraction patterns. High resolution transmission electron microscopy (HRTEM) was also done on a few samples.

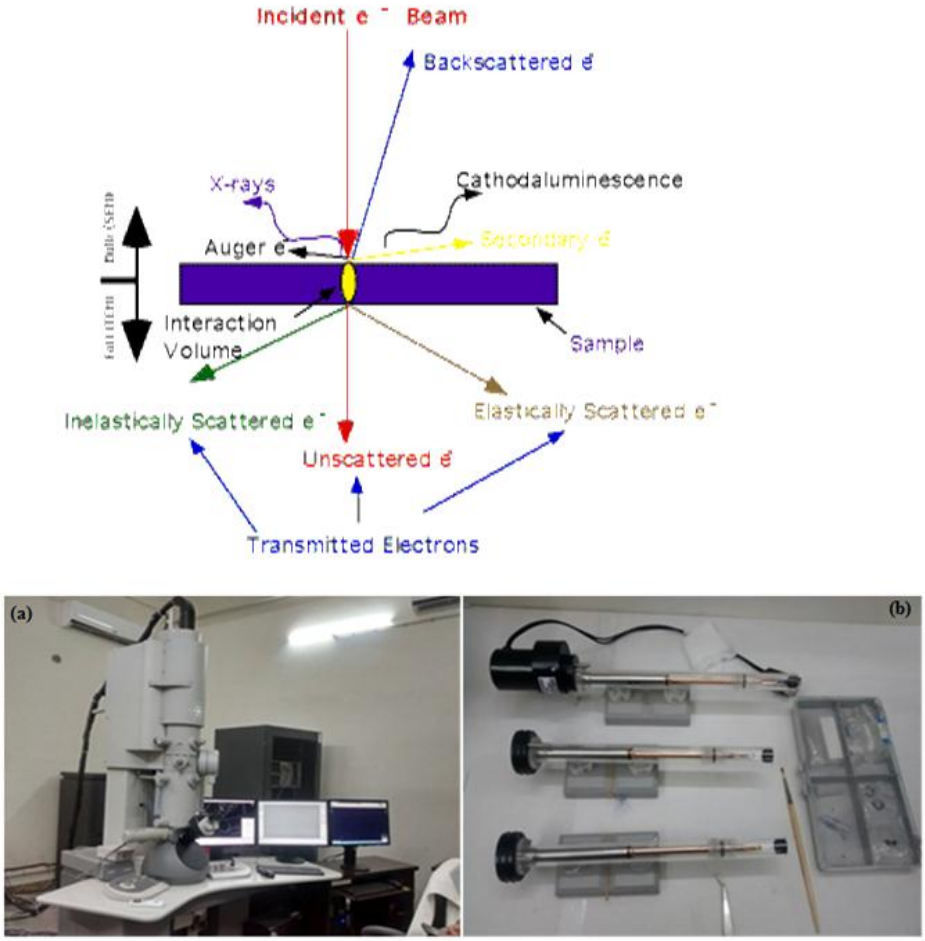

Figure 2. 6: Mechanism (above), experimental setup and Grid (below) of TEM

2.4.5 Field Emission Scanning Electron Microscopy (FESEM)

A field-emission cathode in the electron gun of a scanning electron microscope provides narrower probing beams at low as well as high electron energy, resulting in both improved spatial resolution and minimized sample charging and damage. Under vacuum, electrons generated by a Field Emission Source are accelerated in a field gradient. The beam passes through Electromagnetic Lenses, focusing onto the specimen. As a result of

this bombardment different types of electrons are emitted from the specimen. A detector catches the secondary electrons and an image of the sample surface is constructed by comparing the intensity of these secondary electrons to the scanning primary electron beam. Finally the image is displayed on a monitor. Mechanism of FESEM is shown in Fig. 2.7. FESEM produces clearer, less electrostatically distorted images with spatial resolution down to 1-1/2 nm. That's 3 to 6 times better than conventional SEM. Smaller-area contamination spots can be examined at electron accelerating voltages compatible with Energy Dispersive X-ray Spectroscopy and high quality, low voltage images are obtained with negligible electrical charging of samples. The high-resolution reached by FESEM (~2 nm) allows the study of very small microstructural details, morphology analysis (particles shape and size), fracture studies, interface behavior, quantitative and qualitative elemental analysis, also grain orientation, texture and phase identification can be done.

Sintered pellets were polished using emery papers of grade 1/0, 2/0 and 3/0 (Sia, Switzerland) successively followed by polishing on a velvet cloth with diamond paste of grade1/4-OS-475 (HIFIN). Then, these were etched thermally at 1200 °C for 1 hr. The micrographs were recorded using, QUANTA 200 F, Field Emission Scanning Electron Microscope (FESEM).

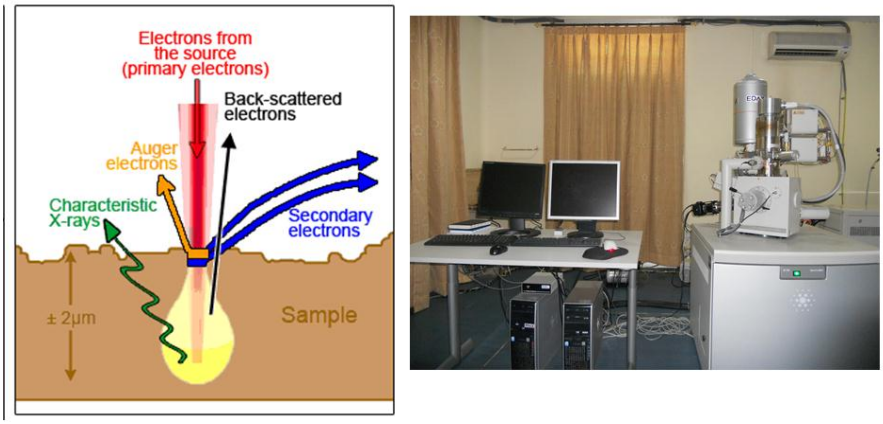

Figure 2.7: Mechanism (left) and experimental setup of FESEM (QUANTA 200 F) (right) [Ref: http://infohost.nmt.edu]

2.4.6 X-ray Photoelectron Spectroscopy

X-ray photoelectron spectroscopy (XPS) is a surface-sensitive quantitative spectroscopic technique that measures the elemental composition at the parts per thousand range, empirical formula, chemical state and electronic state of the elements that exist within a material. XPS spectra are obtained by irradiating a material with a beam of X-rays while simultaneously measuring the kinetic energy and number of electrons (intensity) that escape from the top 0 to 10 nm of the material being analyzed (Fig. 2.5). XPS requires a high vacuum (P~10^{-8} millibar) or ultra-high vacuum (UHV; P < 10^{-9} millibar), although a current area of development is an ambient-pressure XPS, in which samples are analyzed at pressures of a few tens of millibar. XPS is a non-destructive surface chemical analysis technique that can be used to analyze the surface chemistry of a material in its as-received state, or after some treatment, for example: fracturing, cutting or scraping in air or UHV to expose the bulk chemistry, ion beam etching to clean off some or all of the surface contamination (with mild ion etching) or to intentionally expose deeper layers of the sample (with more extensive ion etching) in depth-profiling XPS, exposure to heat to study the changes due to heating, exposure to reactive gases or solutions, exposure to ion beam implant, exposure to ultraviolet light. XPS is also known as ESCA (Electron Spectroscopy for Chemical Analysis). XPS is routinely used to analyze inorganic compounds, metal alloys, semiconductors, polymers, elements, catalysts, glasses, ceramics, paints, papers, inks, woods, plant parts, teeth, bones, medical implants, bio-materials, ion-modified materials and many others. An Amicus XPS setup was used to performed elemental analysis and chemical state of the compositions and is shown in Fig. 2.8.

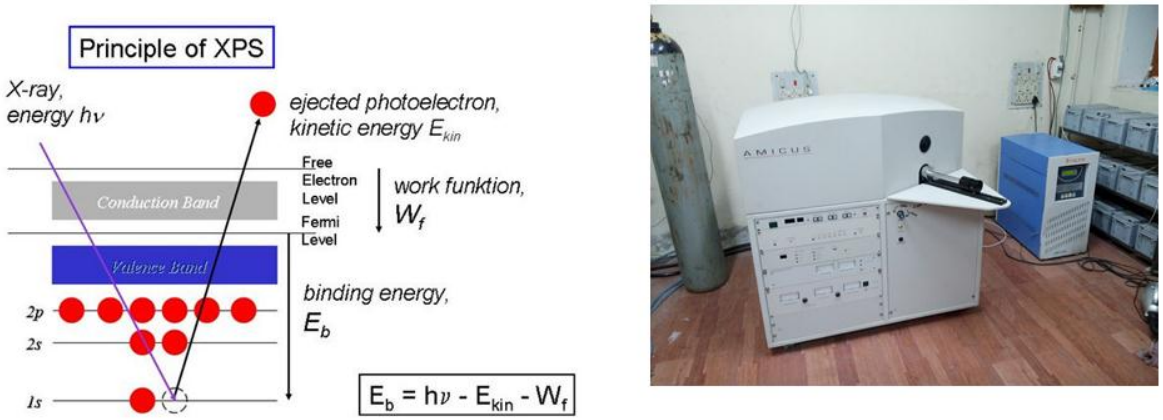

Figure 2.8: Mechanism (left) and experimental setup (Amicus) of X-ray photoelectron spectroscopy

2.5 Electrical Properties

The electrical behaviours of the compositions was studied by following two techniques:

2.5.1 Conductivity Spectroscopic Technique

Electrical conductivity spectroscopy is a most powerful technique for the investigation of electrochemical properties. To tailor the properties of ion conducting materials understanding of their ion dynamics is necessary. Thus, the different groups and authors have tried various approaches to understand the ion dynamics in a number of systems, such as glasses, polymers, semiconductors, nano-composites and poly-crystals etc., and succeed to explore mechanism of conduction [63]–[65]. The ion dynamics can be extracted with the help of either conductivity spectra [66] or modulus spectra [67]. In the former description, the real part of ac conductivity, σ' of ionic conductor could be described in term of Jonscher's power law:

$$\sigma' = \sigma_{dc} + A\omega^n = \sigma_{dc}\left[1+\left(\frac{\nu}{\nu_p}\right)^n\right] \qquad 2.4$$

Here, factor *A* is a constant and depends on several parameters among which absolute temperature, number of vacant sites in the material and the average hopping length between randomly distributed localized sites are the most important [68], [69]. The above

expression consists of two parts: (i) frequency independent part commonly known as dc conductivity, σ_{dc} and (ii) frequency dependent ac component. ν_p is the cross over frequency from dc to the dispersive conductivity region and n is power-law exponent represent the electric relaxation behavior of the material with value generally smaller than unity. Almond and West proposed crossover frequency as hopping frequency in their work[33]. The hopping frequency, w_H, can be also correlated with dc conductivity through Nernst-Einstein relation

$$\sigma_{dc} = en_c\mu = \frac{n_c e^2 \gamma \lambda^2}{kT} \nu_H \qquad 2.5$$

where n_c is the concentration of the mobile charge carriers, μ is their mobility, e is the electronic charge, γ is a geometrical factor for ion hopping, λ is the hopping distance, and k is Boltzmann's constant. The above equation can be used to estimate the charge carrier concentration and its variation with temperature. It has been proven that conductivity spectra of ion conducting materials at different temperature follow the scaling law known as the time temperature superposition principle (TTSP). It means, for a material, the conductivity isotherm can be superimposed to a single curve using appropriate scaling parameters with respect to conductivity and frequency. This principle can be mathematically expressed as [63].

$$\frac{\sigma'(\omega)}{\sigma_{dc}} = F\left(\frac{\nu}{\nu_s}\right) \qquad 2.6$$

where, F is a temperature independent function and ν_s is a temperature dependent scaling parameter. In the literature various types of scaling models have been proposed by different workers such as Summerfield scaling [70], Roling et al. scaling [71], Sidebottom scaling [72], Baranovskii and Cordes scaling [73] and Ghosh scaling [63]. All the models differ with respect to each other by the choice of scaling parameter ω_s. In Summerfield

scaling $\sigma_{dc}.T$, in Roling et al. scaling $\sigma_{dc}.T/x$ or $\sigma_{dc}.T/n_c$, in Sidebottom scaling $\sigma_{dc}/(\varepsilon_o\Delta\varepsilon)$, in Baranovskii and Cordes scaling $\sigma_{dc}.T/T^{\alpha}$ and in Ghosh scaling ω_H is chosen as the scaling parameter. Among above scaling Ghosh scaling is widely applicable because of automatic consideration of changes in permittivity and the Haven ratio [63].

In polycrystalline ceramic system, conductivity relaxation occurs due to grain, grain boundary, and electrode-specimen interface contributions. The conductivity spectra of these materials consist of two plateaus and two dispersion regions in the absence of electrode polarization [74]. The first plateau in a low-frequency region represents the total or the bulk conductivity (σ_{dc}) and the successive dispersion region is due to the combined effect of the grain conductivity and grain-boundary dielectric relaxation processes. The second plateau after this dispersion region corresponds to the grain contribution to the bulk conductivity. The successive dispersion after second plateau, in the high frequency regime, is due to the dielectric contribution of the grain relaxation. In the absence of electrode polarization, electrical conductivity can be measured in two dispersion regions in their frequency dependent conductivity spectra. The low-frequency (or frequency independent region) plateau represents the dc conductivity (let us say dc conductivity σ_{dc}) followed by a dispersion region caused by the combined effect of grain conductivity and grain-boundary dielectric relaxation processes. The dc conductivity provides only quantitative measures of the materials and provides less information of the entire dynamic behavior of the sample. Thus a second plateau is observed after this dispersion regime representing the grain contribution to the total conductivity. Dispersion after this plateau, in the high frequency regime, represents the dielectric contribution of the grain relaxation. Conductivity spectra in two parts: the frequency-independent part assigned to the dc conductivity caused by the random motion of the mobile charge carriers, and the frequency-dependent part (dispersion regime) assigned to the ac conductivity caused by

the hopping motion of the charge carriers in grains and grain boundaries. AC conductivity is used for material properties such as bulk conductivity, surface, grain boundary effect, ionic transport and double layer formation at the electrode/electrolyte interface.

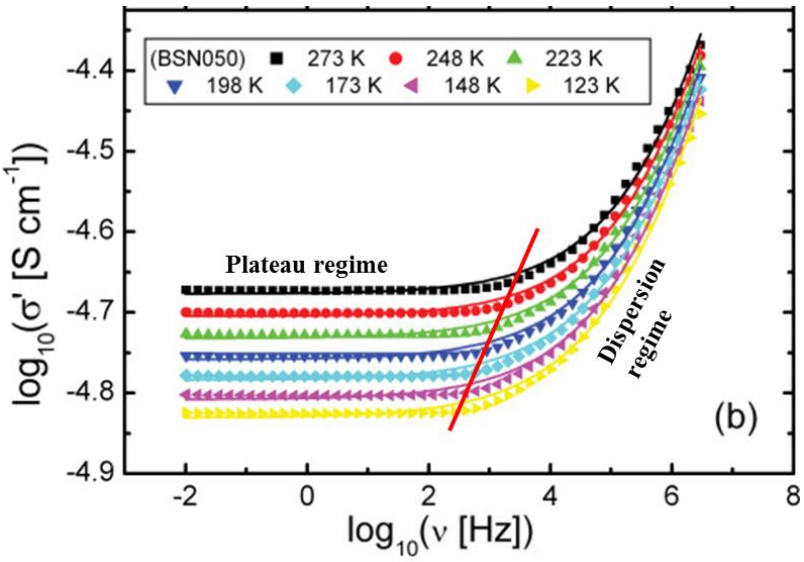

Figure 2.9: Conductivity spectra of a polycrystalline material [Singh et al. (2011)]

2.5.2 Impedance Spectroscopic Technique

Overall dielectric and electrical properties of polycrystalline electronic ceramics have contributions from (i) bulk or grains (ii) grain boundaries and (iii) electrode specimen interface or electrode polarization. In order to understand the electrical behavior and to tailor the useful properties, it is necessary to separate these contributions [Irvine, et al. (1990)]. Impedance analysis has emerged as a powerful and simple tool to separate the various contributions present in the electrical/ dielectric properties of electronic ceramics [75], [76]. It is useful in the studying defects, microstructure, surface chemistry and electrical conductivity of materials, including dielectrics, ionic conductors and adsorbate-adsorbent interface. The AC response of the materials can be expressed by any of the four basic formalisms. These are complex impedance (Z^*), admittance (Y^*), electric modulus (M^*) and permittivity (ε^*) jointly referred to as immittance functions. These are related to one another, as follows:

$$Z^* = Z' - iZ'' = \frac{1}{i\omega C_0 \varepsilon^*} \quad 2.7$$

$$Y'' = Y' + iY'' = i\omega C_0 \varepsilon^* \quad 2.8$$

$$M^* = M' + iM'' = \frac{1}{\varepsilon^*} \quad 2.9$$

$$\varepsilon^* = \varepsilon' - i\varepsilon'' \quad 2.10$$

Correlation among various parameters can be inscribed as follows:

$$D = \tan\delta = \frac{\varepsilon''}{\varepsilon'} = \frac{M''}{M'} = \frac{Y'}{Y''} = \frac{Z'}{Z''} = \frac{\sigma'}{\sigma''} \quad 2.11$$

$$Z' = \frac{D^2}{G \cdot (1 + D^2)} \ , \ Z'' = \frac{Z'}{D} \quad 2.12$$

$$\sigma' = \omega\varepsilon_0\varepsilon'' \text{ and } \sigma'' = \omega\varepsilon_0\varepsilon' \quad 2.13$$

where, ω is the angular frequency, ω=2πf of applied electric field, 'f' being the frequency in cycles/sec, C_0 is the geometrical capacitance. For electronic ceramics Z*, Y* and M* are mostly used. Two types of plots may be generated (1) Complex plane plots, e.g. Z'' vs. Z' and M'' vs. M' plots and (2) Spectroscopic plots Z'' or M'' vs. log ν plots. For complex plane immittance analysis Z'' and Z' or M'' and M' has measured over a range of frequencies and plotted as Z'' vs. Z' or M'' vs. M'. If a polycrystalline ceramic has contributions from grains, grain boundaries and electrode, then each of these contributions can be represented by a circuit element containing R and C connected in parallel. The sample can therefore be represented by an equivalent circuit containing three parallel RC circuit elements connected in series as shown in Fig. 2.10. Cole-Cole plot (Nyquist plot) is the most widely used to communicate frequency response information of a system by complex impedance function $Z^*(\omega) = Z'(\omega) - jZ''(\omega)$, where $Z'(\omega)$ and $Z''(\omega)$ are the real and imaginary parts of $Z^*(\omega)$.The real (Z') and imaginary (Z'') part of the total impedance of equivalent circuit is defined as

$$Z' = \frac{R_g}{(1+\omega R_g C_g)^2} + \frac{R_{gb}}{(1+\omega R_{gb} C_{gb})^2} \qquad 2.14$$

$$Z'' = R_g \frac{\omega R_g C_{gb}}{(1+\omega R_g C_g)^2} + R_{gb} \frac{\omega R_{gb} C_{gb}}{(1+\omega R_{gb} C_{gb})^2} \qquad 2.15$$

where, R_g and C_g are the bulk (grain) resistance and capacitance, respectively, and R_{gb} and C_{gb} are the corresponding quantities for interfacial boundary (grainboundary). The relative position of the two arcs in a complex plane can be identified by frequency. The arc of bulk generally lies in the frequency range higher than that of interfacial boundary since the relaxation time for the interfacial boundary is much larger than that for the bulk crystal. Hence, when the bulk resistance (R_g) is much lower and the resistance in the equivalent circuit is dominated by the interfacial boundary resistance (R_{gb}), the arc of bulk (grain) may be masked in the limited frequency range. R_g, R_{gb} and R_{el} represent the resistive contributions of grains, grainboundaries and electrode polarization process while C_g, C_{gb} and C_{el} represent their corresponding capacitive contributions, respectively. In complex plane impedance and modulus analysis, one observes three semicircular arcs with their centers on the real axis if each of the above three contributions has a single value of relaxation time as shown in Fig. 2.10. Relaxation time τ which is equal to the inverse of the angular frequency, ω at which the relaxation peak occurs, is given by the RC product i.e.

$$\tau = 1/\omega = RC \qquad 2.16$$

The equations for the real axis intercepts for various Immittance functions in complex plane plots are given by Hirose and West. The intercepts of the arcs with the real axis ($Z^{/}$) give the resistive contributions R_g, R_{gb} and R_{el} in the impedance plots. The intercepts with $M^{/}$ axis in modulus plots are inversely proportional to the capacitive contributions (C_o/C_g, C_o/C_{gb} and C_o/C_{el}). The value of the capacitance from the impedance plots and resistance from the modulus plots can be obtained from the frequency of the peak point in the arc

where the relation $\omega RC = 1$ is satisfied. Frequency increases in opposite direction in complex plane impedance and modulus plots. The electrode polarization processes being most sluggish appear in the lowest frequency range followed by grainboundaries in the intermediate frequency range and bulk or grains contribution appears in the highest frequency range in the impedance plots. If any of the above contributions has a distribution of relaxation times rather than a single value, then one observes a depressed circular arc with its centre below the Z' or M' axis. The angle,α, which the line joining the origin to the centre of circle makes with real axis is a measure of distribution of relaxation times of that contribution.

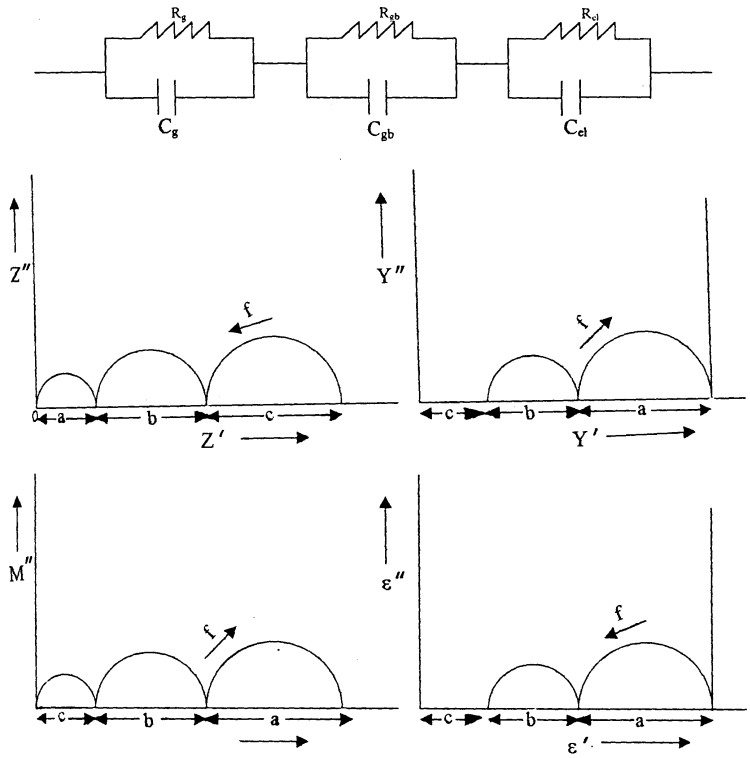

Figure 2.10: Equivalent circuit for a polycrystalline ceramic sample and corresponding frequency response in the complex plane plots [Ref: R. Gerhardt, 1994].

The actual number of arcs appearing in the complex plane plots also depends on the ratio of various times constants. An electronic ceramic having negligible value of electrode-specimen interface contribution (ohmic contact), can be represented by two parallel RC elements connected in series. Bulk and grainboundary conductivities σ_g and

σ_{gb}, can be calculated respectively, using relations $\sigma_g = (1/R_g)\cdot(t/A)$ and $\sigma_{gb} = (R_g C_b / R_{gb} C_{gb}).\sigma_g$ with C being the respective capacitances. These resistances and capacitances (i.e. R_g, R_{gb}, C_g and C_{gb}) can be estimated from the best fit of the Cole-Cole plots at various temperatures. Whether a full, partial or no semi-circle is observed in a Cole-Cole plot, depends on the strength of relaxation, value of distribution parameters and the experimentally available frequencies. Strength of relaxation is defined as $\varepsilon_S / \varepsilon_\infty$ where ε_S is the value of static dielectric constant as $\omega \rightarrow 0$ and ε_∞ is the dielectric constant as $\omega \rightarrow \infty$ i.e. at optical frequencies. Therefore, it is not surprising that certain function is favoured on other depending on whether the material being studied is insulating, semiconducting or conducting [75]. It is clear from above discussion that impedance plots highlight circuit element (contribution) with large resistance (grainboundaries and electrode-specimen interface) while the modulus plots highlight the contribution with minimum capacitance (bulk contribution) [75]. We usually see three-arc responses which are related to the bulk, grain boundary and electrodes relaxations. If the frequency range is not limited, we may see every process which is related to this electrochemical reaction by impedance spectroscopy. However, due to experimental limitations, we only see some parts of the whole response depending on the temperature. For modelling of this impedance spectrum, an equivalent circuit was made which is suitable for the system. When we have a perfect semicircle, a capacitor can be used in the equivalent circuit model. However, in real circumstances, the arc is often depressed and this leads to the necessity of a constant phase element (*CPE*). In this case, a constant phase element (*CPE*) was used instead of a pure capacitor for modelling equivalent circuit to real impedance data. A constant phase element is equivalent to a distribution of capacitors in parallel and it arises due to the microstructural inhomogeneities within the sample [28]. The capacitance of CPE is given by the relation $C = Q^K R^{(1-K)/K}$, where the parameter k estimates the deviation from ideal

capacitive behaviour. The values of K is zero for the pure resistive case and unity for the pure capacitive one. The values of K are calculated from the slope of the corrected modulus, log|Z| vs log frequency plots. At high frequencies, the corrected modulus is dominated by the contribution of the imaginary part of the impedance. The corrected modulus approaches zero, according to $|Z|_{adj} \approx f^{-K}$. Thus, the slope on a logarithmic plot has a value of –K at high frequencies. Usually, the value of K determines the roughness of the surface, but the surface roughness gives only the minute changes. But in the present case, K changes with the temperature, which can be attributed to the formation of ionic charge carriers in comparison to the deformation in the lattice.

For electrical measurements, in present investigations, sintered pellets were polished with the help of emery papers of grade 1/0, 2/0 and 3/0 (Sia, Switzerland) and high temperature Ag paste was applied on both the polished surfaces of the pellets. Polished pellets were dried in oven at 100 °C for 10 minutes and then cured at 700 °C for 20 minutes.

AC impedance measurements (the value of real and imaginary parts of impedance i.e. $Z^{/}$ and $Z^{//}$) of different samples were carried out on electroded pellets using two probe method in the frequency range 20 Hz to 1 MHz and at an interval of 25 °C in the range 200 – 800 °C in air using a Wayne Kerr 6500 P impedance analyzer. AC Impedance measurements were measured in a PID controlled electric furnace with the help of sample holder. The measurement setup is shown in Fig. 2.11.

Figure 2.11: Computer controlled automated impedance analyzer setup along with sample holder and furnace (6500 P Wayne Kerr, UK)

2.6 Analysis Techniques

2.6.1 Rietveld Refinement technique

In order to understand the properties of oxide ion conductors and to improve ionic mobility, their structural information has to be known more precisely. Among many analysis tools, the more effective and common method to do this is the X-ray diffraction. R.M. Rietveld has firstly developed a structure profile refinement method for powder diffraction data of X-ray and Neutron radiation. The Rietveld refinement method creates an effective separation of these overlapping data, thereby allowing an accurate determination of the structure. The height, width and position of these reflections can be used to determine many aspects of the material's structure.In the Rietveld refinement the least square refinement is carried out until the best fit is obtained between the entire observed powder diffraction patterns taken as a hole and entire calculated pattern based on simultaneously refined model for crystal structure. Therefore, applying the Rietveld refinement method to a powder diffraction pattern, it is possible to obtain much more information about structure factors of the material.

The shape of a powder diffraction reflection is influenced by the characteristics of the beam, the experimental arrangement, and the sample size and shape. In the case of monochromatic neutron sources the convolution of the various effects has been found to result in a Gaussian shape. If this distribution is assumed then the contribution of a given reflection to the profile y_i at position $2\theta_i$ is:

$$y_i = I_k \exp\left[\frac{-4\ln(2)}{H_k^2}(2\theta_i - 2\theta_k)^2\right] \qquad 2.17$$

where, H_k is the full width at half peak height (full-width half-maximum), $2\theta_k$ is the centre of the reflex, and I_k is the calculated intensity of the reflex (determined from the structure factor, the Lorentz factor, and multiplicity of the reflection). At very low diffraction angles the reflections may acquire an asymmetry due to the vertical divergence of the beam. Rietveld used a semi-empirical correction factor, A_s to account for this asymmetry

$$A_s = 1 - \left[\frac{sP(2\theta_i - 2\theta_k)^2}{\tan\theta_k}\right] \qquad 2.18$$

The width of the diffraction peaks are found to broaden at higher Bragg angles. This angular dependency was originally represented by

$$H_k^2 = U\tan^2\theta_k + V\tan\theta_k + W \qquad 2.19$$

where, *U, V* and *W* are the half width parameters and may be refined during the fit. The principle of the Rietveld Method is to minimize a function *M* which analyzes the difference between a calculated profile y(calc) and the observed data y(obs). Rietveld defined such an equation as:

$$M = \sum_i W_i \left\{ y_i^{obs} - \frac{1}{c} y_i^{calc} \right\}^2 \qquad 2.20$$

where, W_i is the statistical weight and c is an overall scale factor such that $y^{calc} = cy^{obs}$. In the present thesis, Rietveld refinement was carried by using 'Fullprof' program.